Eur Biophys J (2010) 39:457–468
DOI 10.1007/s00249-009-0430-4

ORIGINAL PAPER

Recombinantly produced hydrophobins from fungal analogues as highly surface-active performance proteins

Wendel Wohlleben · Thomas Subkowski · Claus Bollschweiler · Bernhard von Vacano · Yaqian Liu · Wolfgang Schrepp · Ulf Baus

Received: 14 November 2008 / Revised: 20 February 2009 / Accepted: 23 February 2009 / Published online: 17 March 2009

Abstract Hydrophobins are available from natural resources only in milligram amounts. BASF succeeded in a recombinant production process, up-scaled to pilot plant production in kilogram scale. Strain and protein optimization by modulation of gene expression and generation of fusion proteins finally leads to two class I hydrophobins called H*Protein A and H*Protein B. By analytical ultracentrifugation, we confirm that the self-association of H*Proteins in solution is governed by their sequence, because oligomerization is induced by the same mechanisms (pH $>$ 6, temperature $\gg$ 5°C, concentration $>$ 0.2 mg/ml) as for the well-known native hydrophobins SC3 and HFB II. Additionally, we established the triggering of structure formation by bridging with divalent ions and the stabilization of dimers and tetramers by monovalent ions or surfactants. This interplay with surfactants can be exploited synergistically: The capacity for emulsification of a 300 ppm standard surfactant solution is boosted from 0 to 100% by the addition of a mere 1 ppm of our new hydrophobins, with H*Protein A and H*Protein B having specific application profiles. This astonishing performance is rationalized by the finding that the same minute admixtures enhance significantly the interfacial elastic modulus, thus stabilizing interfaces against coalescence and phase separation.

Keywords Hydrophobin · Recombinant · Self-association · Analytical ultracentrifugation · Interface elasticity · Emulsion

Abbreviations

PCR	Polymerase chain reaction
LB medium	Lysogeny broth medium
LAS	Linear alkylbenzene sulfonate
AUC	Analytical ultracentrifugation

Introduction

Hydrophobins are small proteins of about 100 aa which are characteristic for filamentous fungi (Linder et al. 2005; Sunde et al. 2008). The major biological function is the reduction of the surface tension of water by secreted hydrophobins, allowing fungi to escape an aqueous environment, as well as the hydrophobization of spores facilitating improved dispersal of the conidiospores (Bell-Pedersen et al. 1992; Ma et al. 2006; Wessels 2000; Wosten et al. 1999).

Furthermore several hydrophobins are involved in the attachment of pathogenic fungi to plant surfaces (Hamer

AUC&HYDRO 2008—Contributions from 17th International Symposium on Analytical Ultracentrifugation and Hydrodynamics, Newcastle, UK, 11–12 September 2008.

Electronic supplementary material The online version of this article (doi:10.1007/s00249-009-0430-4) contains supplementary material, which is available to authorized users.

W. Wohlleben (✉) · B. von Vacano · Y. Liu · W. Schrepp
Polymer Physics Research, BASF SE,
67056 Ludwigshafen, Germany
e-mail: wendel.wohlleben@basf.com

T. Subkowski · C. Bollschweiler
Fine Chemicals Research, BASF SE,
67056 Ludwigshafen, Germany

U. Baus
New Technologies, BASF SE, 67056 Ludwigshafen, Germany
e-mail: ulf.baus@basf.com

and Talbot 1998; Lugones et al. 1999; Whiteford and Spanu 2002).

Some fungi contain more than one hydrophobin, e.g. *Schizophyllum commune*, *Coprinus cinereus*, *Aspergillus nidulans*, *Agaricus bisporus*, *Pleurotus ostreatus*, involved in different stages of fungal growth, morphogenesis and development (Kershaw and Talbot 1998; Ma et al. 2007; Penas et al. 2002; Van Wetter et al. 2000).

Even under in vitro conditions the proteins self-assemble into an amphipathic monolayer at hydrophilic or hydrophobic surfaces as well as interfaces (e.g. air/water, oil/water, air/cell wall). In this process the monomers of hydrophobin aggregate spontaneously to oligomers and finally to a fully covered area, resulting in an inversion of the surface polarity (e.g. hydrophilic Teflon® or hydrophobic glass; de Vocht et al. 1998; Lumsdon et al. 2005).

The sequence similarity between different hydrophobins is quite low except for a characteristic pattern of eight cysteine residues that form four intramolecular disulfide bonds (Kwan et al. 2008; Wessels 1994, 1997).

Two major classes of hydrophobins are distinguished by their hydropathy and the spacing between the cysteine residues (Wessels 1994). Furthermore class I hydrophobins show a higher stability versus solvents and detergents: even boiling in a 2% SDS solution is acceptable for a short period of time. Only formic acid or trifluoroacetic acid are able to dissociate the protein layer. In contrast, a class II hydrophobin monolayer is significantly less stable and can readily be dissolved by SDS or 60% ethanol (Wessels 1997).

The physicochemical properties of a few hydrophobins, especially their self-assembly and structure formation at interfaces, have been characterized (Corvis et al. 2006; de Vocht et al. 2002; Ma et al. 2008; Stroud et al. 2003; Wang et al. 2004). For hydrophobin SC3, the self-association in solution was found to increase with higher temperature and higher pH, with an association scheme monomer–dimer–tetramer–agglomerates (Wang et al. 2004). Due to the enormous colloidal heterogeneity with dimers and large agglomerates in coexistence under certain conditions, non-fractionating characterization techniques such as dynamic light scattering (DLS) tend to indicate stronger association of SC3 with several 100 nm large agglomerates at lower concentrations already (Corvis et al. 2006). Applications as colloid stabilizer and wetting agent were tested successfully for SC3 and HFB II, with an industrial focus on Teflon and Kevlar (Lumsdon et al. 2005). Many industrial applications of hydrophobins have been discussed (Hektor 2005; Linder et al. 2005; Wosten 2001), but without a reliable protein source none could be commercialized.

Hydrophobins are available from natural resources only in milligram amounts. BASF succeeded in a recombinant production process based on the generation of a fusion protein. The optimal approach was a combination of the hydrophobins of *A. nidulans* and highly expressed proteins in *E. coli* as the N-terminal part of the fusion protein. Various fusion partners have been evaluated and the focus of this paper are two fusion proteins (H*Protein A and H*Protein B) consisting of the class I hydrophobin DewA and the *Bacillus subtilis* protein yaaD, respectively a truncated form of yaaD. The fermentation and down stream processing was up-scaled to pilot plant production in kilogram scale.

In the present contribution, we evaluate their biophysical properties, namely the structure formation in solution, with a single well-defined liquid–liquid interface, and with multiple interfaces in emulsions. In different experiments, always the same surfactant mixtures were used mimicing realistic laundry and oil field conditions.

We characterize self-association with a more powerful method than previously reported for hydrophobins, namely analytical ultracentrifugation (AUC), which is a fractionating technique and provides absolute data on molar masses or particle sizes. The AUC approach delivers molar mass distributions in any solvent or buffers, and has made eminent contributions to protein interaction studies (Balbo et al. 2005; Demeler 2005; Ohnishi et al. 2008; Stöhr et al. 2008; Walker et al. 1990; Wenta et al. 2008). Specifically the initial aggregation of amyloid fibrils from Alzheimer's β-peptide, a process that is thought to be similar in hydrophobin assembly, has been analysed by AUC (Stöhr et al. 2008; Wiesehan et al. 2008). In the present contribution, AUC experiments compare for selected environments between the H*Proteins and the much studied hydrophobins SC3 and HFB II as benchmarks. As the next step towards application, we subsequently characterize interfacial tension and interfacial elasticity of oil/water oscillating pendant drops with hydrophobins. The interfacial elastic modulus was not determined before, but it is a well-known parameter determining emulsion stability, and hydrophobin structure formation can be expected to be an ideal mechanism for controlling interfacial elasticity. We then proceed from the single interface to the structure formation at multiple interfaces. Standardized oil/water emulsion testing demonstrates that minute amounts of hydrophobin (1 ppm) boost the emulsifying power from 0 to 100% even though 300 ppm of an appropriate technical surfactant is present in both cases.

Materials and methods

Benchmark materials

Hydrophobins SC3 and HFB II were purchased from BioMaDe, Groningen, The Netherlands and VTT Biotechnology,

Espoo, Finland, respectively. Their molar masses are 8.8 kDa (HFB II) and 11 kDa (SC3; de Vocht et al. 1998; Linder et al. 2005).

Cloning of *B. subtilis* yaaD

Using the oligonucleotides 1 + 2 the DNA of yaaD could be amplified in a PCR starting with genomic DNA from *B. subtilis* strain 168 as template DNA.

The obtained fragment of the yaaD coding sequence was surrounded by the *Nco*I and *Bgl*III cleavage side. After purification the DNA fragment was cleaved by *Nco*I/*Bgl*III and transferred to the *Nco*I/*Bgl*III linearized vector pQE-60 (Qiagen).

The vector pQE60yaaD-His6 is the starting point for the generation of the two hydrophobin fusion proteins.

Oligonucleotide 1: GCATCCATGGCTCAAACAGG
Oligonucleotide 2: GCTAGCAGATCTCCAGCCGC

Cloning of H*Protein A *(yaaD-A. nidulans* hydrophobin DewA-His6)

First step was the synthetic generation of the coding sequence of hydrophobin DewA (*A. nidulans* FGSCA4, gene ID 2869124) by the company Geneart, Regensburg, Germany. After cloning in pET17 (Stratagene) the DewA gene could be amplified with the oligonucleotides 3 and 4 (simultaneous introduction of a protease factor Xa cleavage side for a potential cleavage of the fusion partner after expression and purification). The PCR fragment was purified, cleaved by the nuclease *Bam*HI and inserted into the *Bgl*III linearized vector pQE60yaaD-His6 This new vector pQE60yaaD-DewA-His6 could be used for protein expression in *E. coli* using standard technologies (e.g. Qiagen Kit 32903). The molar mass expected and measured of H*Protein A is 47 kDa.

Oligonucleotide 3: 5′-CGAGCTAGGCTCGGATCC*ATTGAAGGCCGC***ATGCGCTTCATCGTCTCTCT**-3′

*Bam*HI *factor Xa side* **DewA**

Oligonucleotide 4: 3′-GCAGCCCATCAGGGATCC**CTCAGCCTTGGTACCAGCGC**-5′

*Bam*HI **DewA**

Cloning of H*Protein B (truncated yaaD-*A. nidulans* hydrophobin DewA-His6)

A fusion protein consisting of the hydrophobin DewA and the 40 N-terminal aa of yaaD was generated by two steps. In a first set of PCRs the truncated yaaD could be amplified with the oligonucleotides 5 + 6 (template DNA pQE60yaaD-DewA-His6) and the appropriate DewA fragment by the oligonucleotides 7 + 8 (template DNA pQE60yaaD-DewA-His6). The two generated fragments were annealed by PCR with the oligonucleotides 5 + 8 (cleavage *Nco*I/*Hin*dIII). The vector pQE60 (truncated yaaD)-DewA-His6 could be used for protein expression in *E. coli* using standard technologies (e.g. Qiagen Kit 32903). The molar mass expected and measured of H*Protein B is 19 kDa.

Oligonucleotide 5: AATTAACCATGGCTCAAACA
Oligonucleotide 6: AAGCGCATGCGGCCTTCAATGACAGCTCCAGCTTCTTCAG
Oligonucleotide 7: CTGAAGAAGCTGGAGCTGTCATTGAAGGCCGCATGCGCTT
Oligonucleotide 8: CTAATTAAGCTTAGTGATGGT

Fermentation

The recombinant *E. coli* strains were incubated in 3 ml LB medium + 100 µg/ml Ampicillin for 8 h at 37°C with 200 rpm. This inoculum was transferred to two 250 ml LB medium + 100 µg/ml ampicillin in 1 l shake flasks and incubated for another 9 h at 37°C at 180 rpm. Finally it was transferred to a 20-l fermentor (13.5 l LB-medium + 100 µg/ml ampicillin), incubated at 37°C and induced by the addition of 140 ml IPTG 100 mM at $OD_{600nm} = 3.5$. After 3 h the fermentation was stopped at an OD_{600nm} of about 150 by cooling down to 10°C and the separation of the biomass (about 1 kg) was achieved by centrifugation.

Purification

Hundred grams of the cell pellet was resuspended in 200 ml 50 mM phosphate buffer, pH 7.5 and dissociated by ultraturrax treatment for 10 min (type T25, Janke & Kunkel), nucleic acids were removed by Benzonase (1 h incubation at room temperature with 500 U Benzonase; Merck, Darmstadt). The cells were disrupted by triple homogenization at 1,500 bar (Microfluidizer M-110EH, Microfluidics Corp.).

After centrifugation (Sorvall RC-5B, 60 min, 4°C, 23,000 g) the supernatant was discarded. The pellet was resuspended and centrifuged three times, each in 100 ml phosphate buffer, pH 7.5 (last step in 100 ml phosphate buffer, pH 7.5 + 1% SDS). After stirring for 60 min at 4°C the combined supernatants were centrifuged for a last time. For further purification 50 ml supernatant was applied on a 50 ml nickel sepharose column (Amersham High Performance, 17-5268-02), equilibrated with 50 mM Tris–HCl, pH 8.0. After washing with 50 mM Tris–HCl, pH 8.0 the protein eluted by 50 mM Tris–HCl, pH 8.0 buffer,

200 mM imidazole. The imidazole was removed by dialysing against 50 mM Tris–HCl pH 8.0.

Co-surfactants and buffers

Two different buffer systems have been used, which were selected to mimic typical laundry applications. They both contain a primary surfactant (emulsifier), to which the hydrophobin proteins under study could be added in ppm amounts. Buffer 1 is composed of a mixture of 100 ppm LAS and 150 ppm Lutensit AS2230, with 1 mM $CaCl_2$ and a pH buffer at pH 7.5 (Na_2HPO_4, KH_2PO_4). Buffer 2 contains 300 ppm of generic C_{10}-alkylsulfate and 3 mM $CaCl_2$, to simulate increased water hardness, buffered at pH 10 (boric acid, KCl, NaOH).

Analytical ultracentrifugation (no interface)

Analytical ultracentrifugation is used to quantify self-association in a hydrophobin solution. AUC was performed at an acceleration of up to 300,000 g (at 60,000 rpm). Under these conditions solutes, proteins or nanoparticles sediment in fractions that are separated according to their size in the range from 0.5 nm (or 500 Da) to 3,000 nm diameter. Simultaneous detection by synchronized optics quantifies the amount and diameter of each fraction independently (Cölfen 2004). Our AUCs are based on Beckman models XL and have been modified at BASF for the online recording of sedimentation with turbidity, interference, Schlieren or UV detection (Mächtle and Börger 2006). Here we use interference optics (Beckman XLI) in order to quantify the potentially present monomer and small oligomers in the presence of larger agglomerates. Especially for the high-salt buffers it is tempting to use an UV absorption optics with a wavelength where only hydrophobins, but not the slowly developing salt gradient are detected. However, the slow scanning speed of the UV optics prohibits their use for the extremely polydisperse hydrophobin distributions, where fast scanning is essential to capture all components. The raw sedimentation signals were evaluated with the c(M) model of Sedfit (Schuck 2005). The chosen rotational speed of 40,000 rpm sets an upper detection limit around 5 MDa, and agglomerates were detected only indirectly by the loss of concentration in the dispersed fraction with lower masses. For ease of comparison, all distributions are shown normalized to their biggest peak.

The AUC evaluation requires the buoyant density of the solute and its frictional ratio. The later is set to $f/f_0 = 1.2$, corresponding to a globular, but not quite spherical shape, in the lack of precise computational models. The more critical parameter, the density of hydrophobin, is determined experimentally in an analytical density gradient with 25% Nycodenz, detected with the synchronized Schlieren optics and evaluated with the calibration refinement of the ideal Hermans–Ende theory (Mächtle and Börger 2006). The density gradient results are reported in the Online Supporting information (Supplementary Figure 12).

Interfacial tension and interface elasticity (single interface)

Interfacial tension at a single, well-defined interface has been measured with the pendant-drop-method: Automated video-analysis of the shape of a drop of one liquid pendant on a capillary immersed in another liquid directly gives access to the interfacial tension (del Rio and Neumann 1997). This also allows the time-resolved measurement of dynamic interfacial tension γ and of interfacial dilatational modulus ε (Myrvold and Hansen 1998), which is determined every $\sim$30 s by inducing a periodic modulation of the drop volume with a frequency of 0.1 Hz and analyzing the response in γ.

Emulsification capacity (multiple interfaces)

Emulsion tests have been run according to the following procedure: 95 ml of buffer solution (without or with hydrophobin addition) has been mixed with $V_{oil} = 5$ ml oil (5 vol%) and shaken five times by hand. After 24 h, the rest oil volume V_{rest} (not emulsified) was measured, giving an emulsification capacity of $(V_{oil} - V_{rest})/(V_{oil})$. Except for palmin, all experiments were performed at room temperature. For palmin, the experiments were performed at 35°C, where palmin is melted.

Results

Production and purification of H*Protein A and B

The two hydrophobin fusion proteins were produced as inclusion bodies which could be easily separated by centrifugation after disruption of the *E. coli* cells. The example of Fig. 1 demonstrates the purification of the fusion protein yaaD-DewA-His6 (H*Protein A) with a molecular weight of about 50 kDa, in reasonable agreement with the expected mass of 46.5 kDa (analogue procedure with H*Protein B). Lower bands represent degradation products of the hydrophobin (western blot, not shown).

Characteristic self-association in solution

In this chapter we evaluate the performance of the two fusion hydrophobin proteins H*Protein A and B compared to the well-known characteristics of hydrophobin

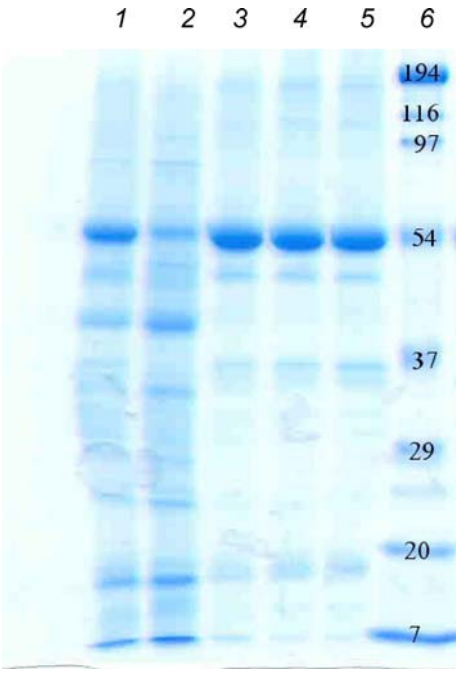

Fig. 1 SDS-PAGE analysis of H*Protein A. *Lane 1* loading sample; *Lane 2* flow through fraction; *Lane 3–Lane 5* elution; *Lane 6* protein molecular marker [MW (kDa) 194, 116, 54, 37, 29, 20, 7]

self-association, and then proceed to examine more involved situations as occurring in specific applications.

Previously it has been pointed out that hydrophobin SC3 shows increased self-association at higher temperature (Wang et al. 2004). When AUC measurements of H*Protein A were performed in aqueous solution at pH 9 and 5°C without further additives, we observe predominantly dimers at 100 kDa, around 10% tetramer at 200 kDa, and a vanishing concentration of hexamer at 300 kDa (Fig. 2). At room temperature under otherwise identical conditions, the mass spectrum is dominated by the tetramer at 200 kDa, and higher oligomers have formed. Agglomeration into larger structures proceeds further at 40°C, where structures beyond 1,000 kDa appear. The AUC result of a dimer at 100 kDa is supported by the monomer mass of 50 kDa found in the SDS-PAGE (Fig. 1), in close agreement with the value of 46.5 kDa expected from the sequence.

Qualitatively the same behaviour is observed for the natural hydrophobin SC3, which had been studied extensively in previous literature (Wang et al. 2004). Even at the concentration of 1.5 mg/ml, which is high in the context of the very pronounced surface activity, the incubation (for 1 h at 5°C) and measurement at 5°C reduces the mass spectrum to the dimer at 22 kDa exclusively (Fig. 2). At ambient temperature, oligomers up to ~100 kDa are present, and at 40°C, agglomeration proceeds further. The experimental resolution does not allow distinguishing between tetramer and higher oligomers for SC3 (Fig. 2). These results confirm previous reports on SC3 self-association (Linder et al. 2005; Wang et al. 2004), but they contradict DLS measurements that reported many orders of magnitude larger agglomerate diameters (Corvis et al. 2006), presumably due to the overscattering cross-section of non-fractionated agglomerates in light scattering.

Although under the conditions tested mainly dimer and higher associations were observed, the monomer of H*Protein A can be detected upon increasing the incubation time at low temperature from 1 to 20 h (Fig. 3). Note that the measurement is also performed at 5°C, because the entire AUC rotor is cooled. Monomers were even detected when incubation was performed first at 40°C (1 h) with subsequent cooling to 5°C. After 1 h at low temperature, the spectrum is still dominated by the dimer, but after 20 h at 5°C, a peak at the monomer mass is observed (Fig. 3), and this mass corresponds within a few per cent to the mass

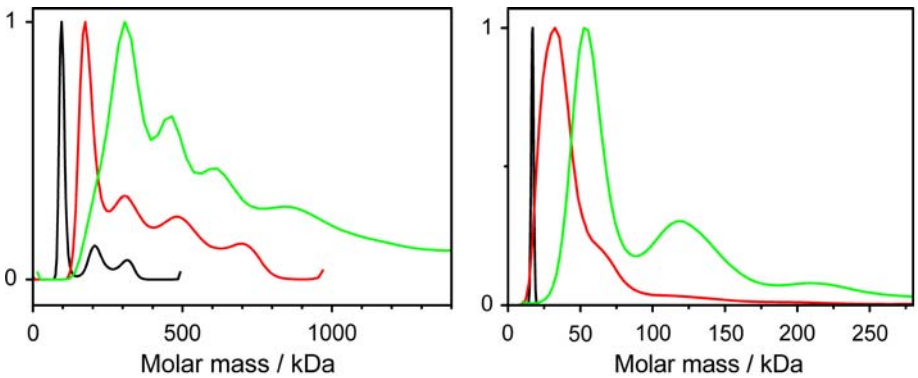

Fig. 2 Similarity of self-assembly, shown by the molar mass distribution (AUC) of H*Protein A (*left panel*) and SC3 (*right panel*), both at 1,500 ppm concentration and pH 9. Even though H*Protein A includes a long fusion partner protein, its self-assembly is determined by the hydrophobin sequence. The dimer of H*Protein A at 100 kDa dominates only at 5°C (*black line*), then forms the tetramer at 25°C (*red line*) and higher oligomers at 40°C (*green line*). The same behaviour is observed for SC3, in good agreement with previous studies (Linder et al. 2005; Wang et al. 2004). Temperatures were equilibrated for 1 h

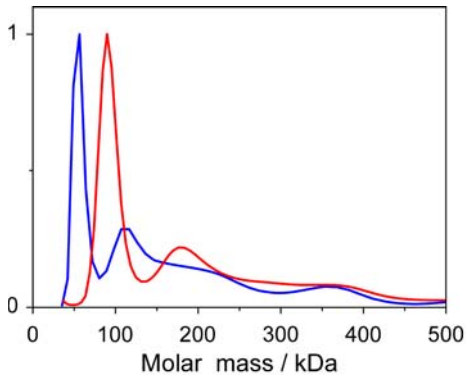

Fig. 3 Molar mass distribution (AUC) of H*Protein A at pH9, 1,500 ppm, after temperature treatment at 40°C for 1 h, then cooling at 5°C for 1 h (*red line*) and for 20 h (*blue line*). The higher oligomers can be reversibly dissociated down to the monomer at 50 kDa

observed with SDS-PAGE (Fig. 1). These results indicate that the agglomeration occuring at 40°C is reversible. Examination of intermediate time steps indicated that the dissociation from high oligomers into monomers takes over 10 h (not shown).

The acidity is another important parameter to control self-association. Even at room temperature, the dimer is made predominant by adjusting to acidic pH (Fig. 4).

The dominance of dimer at room temperature and acidic pH, the slow formation of monomer at low temperatures, and the significantly increased association at elevated temperature or alkaline pH were perfectly comparable for both H*Protein A from BASF and the native hydrophobin SC3 as studied by the Robillard group (Wang et al. 2004). Even though H*Protein A includes a long fusion partner protein, its self-association thus is determined by the hydrophobin sequence.

The composition of the surrounding medium can be drastically different in various potential applications of

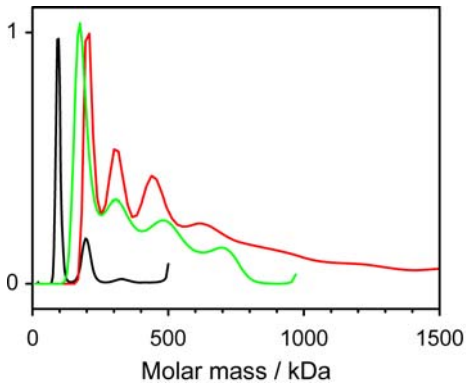

Fig. 4 Molar mass distribution (AUC) of H*Protein A at 1,500 ppm and 25°C with pH variation. Acidic pH induces an effective stabilization of dimer (100 kDa) and tetramer (*black line*), and association is comparable at pH7 (*red line*) or pH9 (*green line*)

hydrophobins, but has not been studied in detail before. Therefore, in the following the presence of surfactants and variations of ionic strength were analysed.

A striking example of the influence of ionic strength is the application of hydrophobins as additive on an oil drilling station, where the aqueous phase is composed of 50% North Sea water and 50% formation water, i.e. water that occurs naturally within the pores of oil-bearing rock. The resulting buffer carries a high salt load of 180 mM Ca^{2+} and 1 M Na^{+} (and other salts in much smaller amounts). At a realistic application temperature of 40°C, the tetramer of H*Protein B is still present under these conditions, but oligomers up to and beyond the 100-mer appear even at acidic pH (results not shown). These may seem like large agglomerates, but they are still rather small compared to the structures formed without Na. With only 3 mM Ca and no other salts at 25°C, strong association and thus structure formation of both H*Protein A and H*Protein B was observed up to the 100-mer, whereas the high-salt system at the same temperature restricts the structure formation to low oligomers. Obviously, charge screening by 1 M monovalent ions significantly reduces the bridging effect of divalent ions.

For the following studies, we suspended the hydrophobins at 25°C and a concentration of 250 ppm in surfactant solutions, in order to mimic the behaviour in a laundry process. The concentration of surfactants in buffer 1 and buffer 2 is 250 and 300 ppm, respectively (Sect. "Materials and methods"). Hard water conditions are reproduced by the addition of Ca^{2+} at 1 and 3 mmol respectively. Surprisingly, at all concentrations tested low molecular weight oligmers were observed as predominant species in these buffers for both H*Protein A and H*Protein B and also for the native HFB II (Figs. 5, 6).

For comparison, the hydrophobins were suspended in the respective buffers without surfactants, and we found that more than 60% of the protein is agglomerated beyond 1 MDa. Also in ultrapure Milli-Q-water without pH control we observe a strong agglomeration beyond the 40-mer for H*Protein B, and a slightly better stability against agglomeration for H*Protein A, where most of the material is below the 20-mer (results not shown).

We conclude that the formation of very large agglomerates is triggered by bridging due to small amounts of divalent ions (Ca^{2+}), and is prevented either by the addition of surfactants ($\sim$0.3 mg/ml in the original buffer composition), or by charge screening with monovalent ions.

As a final axis of variation, self-association is generally expected to be driven by concentration. Using our fusion hydrophobins and AUC mass distribution, we observe a critical concentration of around 250 ppm (Fig. 5). Presumably, the technical surfactant hetero-associates with the biophysical amphiphil and thus keeps apart the proteins

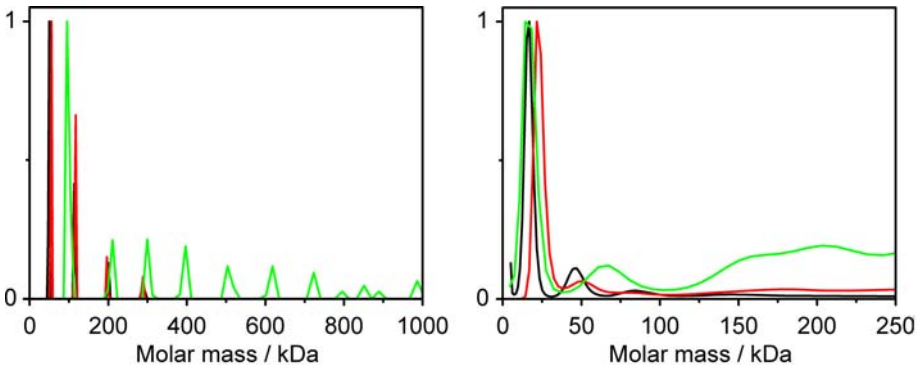

Fig. 5 Molar mass distribution (AUC) of H*Protein A (*left*) and H*Protein B (*right*) in surfactant buffer 1 with protein concentrations of 100 ppm (*black*), 250 ppm (*red*) and 1,500 ppm (*green*). Despite the presence of divalent cations, the hydrophobins do not agglomerate at technically relevant concentrations below 200 ppm, but instead hetero-associate with the added surfactants

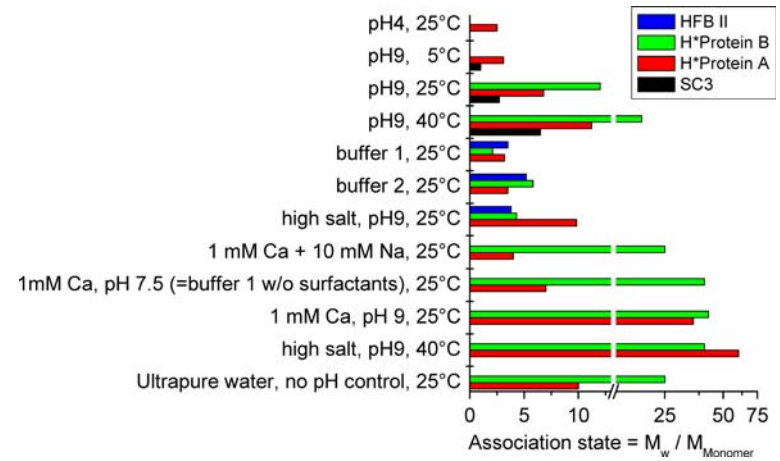

Fig. 6 State of association of different hydrophobins under various suspension conditions with 250 ppm hydrophobin. Note the logarithmic scale after the break in the mass axis. From the molar mass distribution (measured by AUC), the average M_w of the dispersed proteins has been formed and normalized by the known monomer mass

that otherwise would self-associate at lower concentrations already.

All of the above environments are summarized in Fig. 6 together with a few complementary results. The dependence on protein concentration is not represented, but shown for a uniform concentration of 250 ppm. This mass concentration was chosen because the extreme effectiveness in interface activity and emulsification boosting (see below) suggested to measure mass distributions simply at the lowest concentration still provoking good signal to noise ratios. Thus, adjustment was restricted to concentrations below 0.1 mg/ml for the smaller hydrophobins. In the graph, the average molar mass is shown normalized by the known protein mass, such that the state of agglomeration can be compared between the very different hydrophobins. Interestingly, the significantly longer fusion partner of H*Protein A (compared to H*Protein B) does not lead to a dramatic deviation from the structure formation of the native proteins HFB II and SC3 (Fig. 6). H*Protein B self-associates into larger complexes than H*Protein A in ultrapure water with or without pH-control at all temperatures (results not shown). Furthermore, H*Protein B requires significantly higher ionic strength for the reduction of association by charge screening. This shows that electrostatic interactions play a more important role for H*Protein B than for H*Protein A.

One may suspect that some systematics arise from the association being driven by molarity or number concentration, whereas our data compares identical mass concentration. Experimental evidence, however does not support this hypothesis, because the state of association is not systematically lower for H*Protein A as the hydrophobin with the highest monomer mass and hence lowest number concentration, especially not in comparison to the much smaller SC3. The data (Fig. 6) rather suggests that chemical differences determine the different extent to which the hydrophobins follow the common general trends.

In summary of the self-association studies in solution, we confirm that the hydrophobin sequence determines the structure formation in good qualitative accord with a scheme proposed earlier by the Robillard group (Wang et al. 2004), extending themselves the previous scheme by the McCormick group (Stroud et al. 2003). We enlarge the previous knowledge on decisive factors of hydrophobins

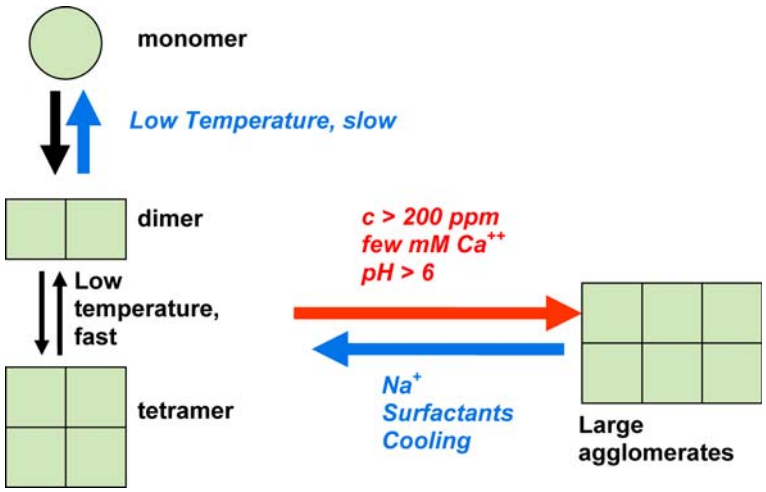

Fig. 7 Scheme of hydrophobin self-assembly in solution without interfaces, building on the results of Robillard (Wang et al. 2004) and McCormick (Stroud et al. 2003) and extended with our results on surfactants and ionic strength

structure formation with our new results on surfactant mixtures and high salt conditions, resulting in the scheme of Fig. 7.

Characterization of hydrophobin as co-emulsifier by interfacial tension and interfacial dilational modulus

Understanding structure formation of hydrophobin in solution is a first step to approach its most remarkable properties unfolding at the interface between two phases. Hydrophobin's ability to reverse the polarity of surfaces by self-assembly in the interface and the astonishingly high surface activity of the protein have already been mentioned (Lumsdon et al. 2005; van der Vegt et al. 1996). The air/water surface tension for example is lowered down to about 30 mN/m in only μM concentrations (Cox et al. 2007). Such surface activity is the driving force for exploring the use of hydrophobin as a novel industrial performance chemical. The application examined in the last sections of this contribution is as co-emulsifier, where hydrophobin shows remarkable effects in smallest concentrations, for example to improve laundering processes.

In almost any practical application of a surface-active material like hydrophobin the knowledge of the equilibrium interfacial properties such as surface tension is not sufficient, but their dynamic behaviour has to be known (Lucassen-Reynders 1981). In this context, it has been shown that hydrophobin exhibits a surface elasticity (interface air/water) by far exceeding other proteins and can therefore be used to efficiently stabilize air bubbles in foams (Cox et al. 2007). Likewise, the dynamic behaviour of interfacial tension and the interfacial elasticity of hydrophobin in a two-phase liquid/liquid system in the presence of generic surfactant will be decisive for its use in emulsification and laundering, and is vital to develop an understanding of structure formation at the interface and the mechanism of hydrophobin action.

The most direct dynamic measurement is the time-resolved determination of the interfacial tension $\gamma_{12}(t)$ between two phases, which gives insight into the time scales of interface organization. The second important dynamic quantity, interfacial elasticity ε, describes the response of an interface to an induced change in the interfacial area A, and is defined as

$$\varepsilon = \frac{\mathrm{d}\gamma_{12}}{\mathrm{d}\ln A} \tag{1}$$

where ε is the interfacial dilatational modulus (also often termed interfacial or surface elasticity) and γ_{12} the interfacial tension between two phases (Lucassen-Reynders 1981). It simply represents the change in interfacial tension induced for a change of relative surface $\mathrm{d}A/A$, mathematically equivalent with $\mathrm{d}\ln A$. A time-resolved measurement of the interfacial tension for a deliberate modulation of the interfacial area A therefore gives access to ε.

Interfacial elasticity measurements thus give information on the rigidity of the interface, which in turn is important for emulsion stability towards rupture and coalescence.

To progress from last section's findings on hydrophobin structure formation in solution and its strong temperature dependency, the next step is to look at the consequences of this behaviour in the organization of the surface-active protein at an interface. Therefore, the dynamic interfacial tension γ and the surface dilatational modulus ε have been measured for a 0.4% solution of H*Protein A in demineralized water at pH 9.5 against the model non-polar solvent octane. The mentioned conditions correspond to a regime where a very strong tendency towards aggregate formation has been shown in solution in the previous section. These data have been obtained at 24, 40, 60 and 80°C and are summarized in Fig. 8. In the interfacial tension γ (Fig. 8a) one can discern a dynamic decrease within the first 100–200 s, reaching an almost constant level afterwards for all

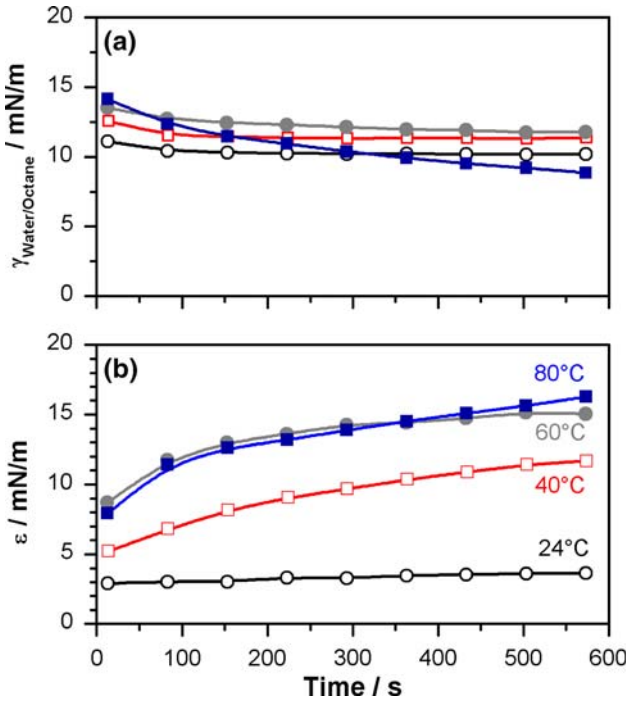

Fig. 8 Dynamic interfacial tension (**a**) and dilatational modulus ε (**b**) between a 0.4% solution of H*Protein A at pH 9.5 versus octane. For the measurement series, the temperature was raised from 24°C (*black open circles*), to 40°C (*red open squares*), 60°C (*grey filled circles*) and finally 80°C (*blue filled squares*)

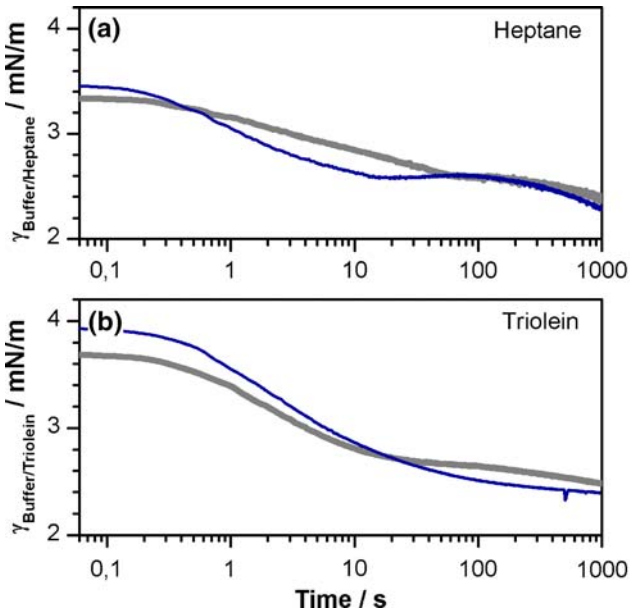

Fig. 9 Dynamic interfacial tension between a surfactant containing aqueous buffer with and without addition of hydrophobin, and two different oily phases heptane (**a**) and triolein (**b**). The interfacial tension of the pure buffer (*grey thick curve*) is compared in both cases with buffer containing 5 ppm H*Protein A (*black solid curve*)

measured temperatures below 80°C. At 80°C, the curve starts at the highest starting value of γ, its decrease continuing well after 200 s reaching the lowest interfacial tension of all the measured data. These findings give a time scale for hydrophobin structure formation at the interface of about 100 s, but the temperature dependence of γ alone is not very conclusive. The changes are, however, much more dramatic looking at the interfacial dilatational modulus ε (Fig. 8b). Here, ε at 24°C almost remains constant at 3–4 mN/m, while it strongly increases for all higher temperatures, reaching values above 15 mN/m in the case of 60 and 80°C. This drastic increase in the "elasticity" of the interface can directly be related to elevated aggregate formation at these temperatures. Also, the initial build-up of ε suggests a time scale of ~100–200 s for structure formation. Again, there is also another, slower process at 80°C, leading to a continuing increase of ε even at later times. This slower process could be related to the formation of the β-sheet II state reported by de Vocht et al. (2002).

Together with the results from the characterization in solution phase this data gives another strong indication that structure formation at the interface is a very important factor for the protein's surface activity.

Although the surface activity of hydrophobin is very high for a protein, it is not in the same league as commercial surfactants. However, its remarkable surface properties also come into play in a synergistic application with a primary surfactant. To study effects of a small amount of hydrophobin in a buffer already containing such a surfactant, the changes in dynamic interfacial tension and interfacial dilatational modulus upon hydrophobin addition have been studied. In order to approach a later application in laundering, such a system has been measured versus two model oily phases heptane and triolein, comparing pure buffer and addition of 5 ppm of H*Protein A. The results are shown in Fig. 9.

In the case of a heptane oily phase (Fig. 9a) the pure buffer (thick grey curve) shows an interfacial tension slowly decreasing from a starting value of ~3.35 mN/m at the earliest measured times to ~2.4 mN/m at 1,000 s. (Note that the interfacial tension is already lowered drastically due to the primary surfactant in the buffer, without it, it would lie in the range of 40 mN/m for heptane.) Upon addition of 5 ppm H*Protein A (black solid curve), the starting interfacial tension is higher, but shows a distinct dynamic decrease intersecting the value of the pure buffer at 0.5 s. From there, it reaches a similar plateau as the pure buffer at ~100 s, but always remains slightly lower. The most dramatic reduction compared to the pure buffer, however, is between 1 and 10 s. In triolein (Fig. 9b), the dynamics of both pure buffer (thick grey curve) and with H*Protein A addition (black solid curve) are more pronounced and showing a greater reduction of interfacial tension over time. In this medium, the effect of H*Protein A co-surfactant is also stronger, leading to an interfacial

tension initially higher by more than 0.2 mN/m, which then becomes markedly lower than in the case of the buffer for times greater 20 s. The previously measured typical equilibration times of hydrophobins at interfaces were 100–1,000 s, in reasonable agreement with our data (Lumsdon et al. 2005).

Depending on the time scales of emulsification, one would infer from this data of dynamic interfacial tension a better emulsification upon addition of hydrophobin, although the effects do not look dramatic. However, one has to keep in mind that these significant changes are the signature of the addition of only 5 ppm of hydrophobin and its remarkable surface activity! Clearly, the dynamics of interfacial tension reveal larger differences than the equilibrium value for larger times.

To look at the system more closely, in a following step the interfacial dilatational modulus ε has been determined for pure buffer, containing surfactant as primary emulsifier, and with addition of 5 ppm of H*Protein A and H*Protein B, as shown in Fig. 10. There, one can see that the surface dilatational modulus for all samples is mostly constant over time, with an indication of some dynamic behaviour in the first 50 seconds in the case of H*Protein A in heptane (Fig. 10a, blue filled squares), H*Protein A in triolein (Fig. 10b, blue filled squares) and H*Protein B in triolein (Fig. 10b, red open squares). Compared to the buffer, both H*Protein A and H*Protein B show an increased ε in heptane (Fig. 10a), while in triolein only H*Protein A shows a higher value. This is summarized in Fig. 10c as a bar graph, containing the average ε for $t > 100$ s. Looking at the significant changes of the surface dilatational modulus upon addition of such low concentrations of hydrophobin, a visible effect on emulsion stability can be expected for experiments, although ε might not be the single determining criterion.

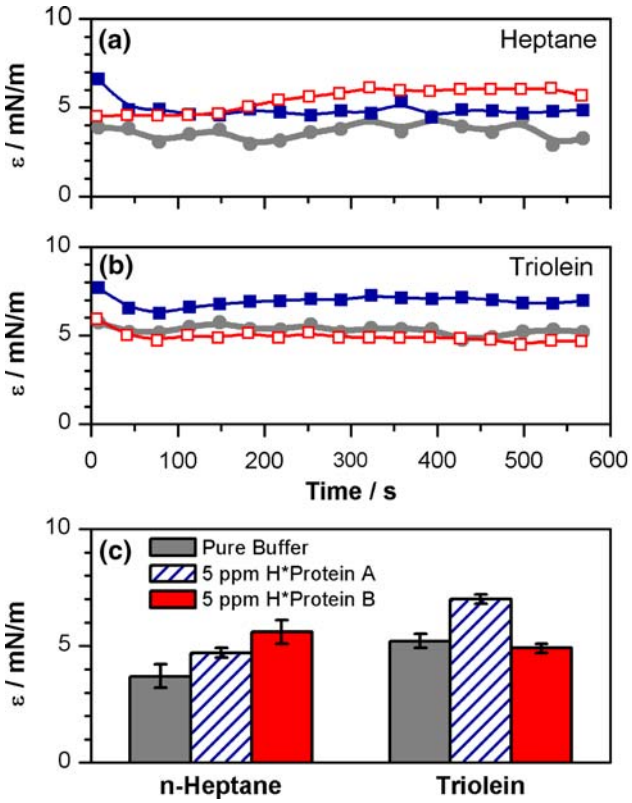

Fig. 10 Interfacial dilatational modulus ε (interfacial elasticity) of a surfactant containing aqueous buffer with and without addition of hydrophobin in heptane (**a**) and triolein (**b**). The interfacial tension of the pure buffer (*grey filled circles*) is compared with buffer containing 5 ppm H*Protein A (*blue filled squares*) and 5 ppm H*Protein B (*red open squares*). The average interfacial dilatational moduli ε are shown in (**c**)

Emulsification characterization of hydrophobin co-emulsifier

Emulsification tests were performed according to the procedure described in the experimental section. For the oily phase, several model substances have been used: heptane, triolein, sunflower oil, olive oil and palmin oil. For each of these phases, the emulsification capacity was determined for pure buffer, addition of 1 and 5 ppm of H*Protein A (Fig. 11b), as well as the same amounts of H*Protein B (Fig. 11c).

For H*Protein A, one can already see a dramatic effect of hydrophobin addition (Fig. 11b): While pure buffer 1 does not emulsify a measurable amount of heptane, 1 ppm of H*Protein A already leads to 40% emulsification, and 5 ppm to a yet higher value of 60%. In triolein, the effect is not as pronounced: increasing the H*Protein A concentration from 0 to 5 ppm leads to an increase of the emulsification capacity from 20 to 40%. In sunflower oil, pure buffer 1 is already capable of emulsifying the complete amount of oil, so an additional effect of hydrophobin cannot be expected. However, if the buffer is changed to a different surfactant and a threefold increased background concentration of $CaCl_2$, this picture changes dramatically: pure buffer 2 is not capable of emulsifying sunflower oil at all under these conditions, but addition of 5 ppm of H*Protein A mitigates this and yields 100% emulsification capacity. Marked increase is also achieved for olive oil and palmin oil, the latter being completely emulsified at 1 ppm of H*Protein A already, compared to 0% for pure buffer 2.

In the case of H*Protein B (Fig. 11c) the results are similar, with even better performance as "efficiency booster" in all cases shown. 1 ppm is already capable of increasing the emulsification capacity of n-heptane in buffer 1 from 0 to 100%! Also, for triolein in buffer 1, 100% emulsification was achieved with 5 ppm H*Protein B. Again, buffer 1 is already capable of completely emulsifying sunflower oil, but buffer 2 fails and needs addition of hydrophobin to achieve this.

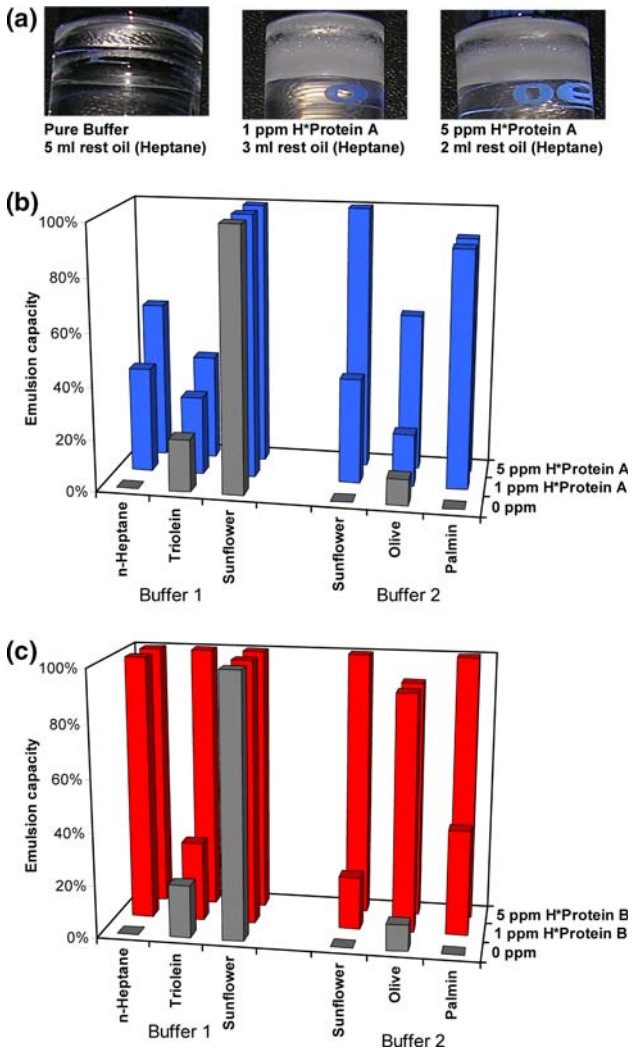

Fig. 11 Effect of H*Protein A (**b**) and H*Protein B (**c**) on emulsification efficiency. Shown is the emulsification capacity of a 95:5 mixture buffer:oily phase for two different surfactant systems (buffer 1 and buffer 2, see text for details). The successful emulsification is directly visible in the **a** photos of a single emulsion series (see Sect. "Materials and methods" for details)

In summary, the emulsification tests show huge effects of hydrophobin addition in ppm amounts, even larger than one might perhaps expect from the findings on interfacial tension characterizations. This proves hydrophobin as novel, attractive industrial performance protein for uses such as laundering. The exact prediction of application test results from the physical characterization, however, needs some further study on the mode of action and structure formation of hydrophobin.

Conclusion

We find that the structure formation and interface activity of the recombinantly produced hydrophobins H*Protein A and H*Protein B is not hindered by the attached fusion protein of comparable sequence length. The dominance of dimer at room temperature and acidic pH, the slow formation of monomer at 5°C, and the much increased association at elevated temperature or alkaline pH are perfectly analogous between the fusion partner hydrophobin H*Protein A and the native hydrophobin SC3 as studied by the Robillard group (Wang et al. 2004). Even though H*Protein A includes a long fusion partner protein, its self-association is determined by the hydrophobin sequence. For the H*Proteins, but also for HFB II and SC3, we find that dimer and tetramer are stabilized by surfactants and monovalent salt. We have thus successfully transferred the unique properties of hydrophobins from a scarce natural product to an industrial scale-up of designed hydrophobins.

Standardized emulsion testing under realistic laundry conditions demonstrates that minuscule amounts of hydrophobin (1 ppm) can boost the emulsifying power from 0 to 100% even though 300 ppm of an appropriate technical surfactant are present. The application tests in emulsion also show that the fusion partner influences the protein performance, because it induces different amounts of emulsion stability boosting for specific oils. This astonishing performance is rationalized by the finding that the same minute admixtures enhance significantly the interfacial elastic modulus, thus stabilizing interfaces against coalescence and phase separation. Being effective in extreme dilution justifies the term "performance protein" for the technical hydrophobins H*Protein A and H*Protein B.

Acknowledgement We thank Monika Page and Werner Wacker for excellent laboratory support.

References

Balbo A, Minor KH, Velikovsky CA, Mariuzza RA, Peterson CB, Schuck P (2005) Studying multiprotein complexes by multisignal sedimentation velocity analytical ultracentrifugation. Proc Natl Acad Sci USA 102:81–86. doi:10.1073/pnas.0408399102

Bell-Pedersen D, Dunlap JC, Loros JJ (1992) The Neurospora circadian clock-controlled gene, ccg-2, is allelic to eas and encodes a fungal hydrophobin required for formation of the conidial rodlet layer. Genes Dev 6(12a):2382–2394

Cölfen H (2004) Analytical ultracentrifugation of nanoparticles. In: Encyclopedia of nanoscience and nanotechnology. American Scientific Publishers, Stevenson Ranch, pp 67–88

Corvis Y, Brezesinski G, Rink R, Walcarius A, Van der Heyden A, Mutelet F, Rogalska E (2006) Analytical investigation of the interactions between SC3 hydrophobin and lipid layers: elaborating of nanostructured matrixes for immobilizing redox systems. Anal Chem 78:4850–4864. doi:10.1021/ac0602064

Cox AR, Cagnol F, Russell AB, Izzard MJ (2007) Surface properties of class II hydrophobins from *Trichoderma reesei* and influence on bubble stability. Langmuir 23:7995–8002. doi:10.1021/la700451g

de Vocht ML, Scholtmeijer K, van der Vegte EW, de Vries OMH, Sonveaux N, Wosten HAB, Ruysschaert JM, Hadziioannou G, Wessels JGH, Robillard GT (1998) Structural characterization of the hydrophobin SC3, as a monomer and after self-assembly at hydrophobic/hydrophilic interfaces. Biophys J 74:2059–2068. doi:10.1016/S0006-3495(98)77912-3

de Vocht ML, Reviakine I, Ulrich WP, Bergsma-Schutter W, Wosten HAB, Vogel H, Brisson A, Wessels JGH, Robillard GT (2002) Self-assembly of the hydrophobin SC3 proceeds via two structural intermediates. Protein Sci 11:1199–1205. doi:10.1110/ps.4540102

del Rio OI, Neumann AW (1997) Axisymmetric drop shape analysis: Computational methods for the measurement of interfacial properties from the shape and dimensions of pendant and sessile drops. J Colloid Interface Sci 196:136–147. doi:10.1006/jcis.1997.5214

Demeler B (2005) UltraScan 9.5—a comprehensive data analysis software package for analytical ultracentrifugation experiments. In: Scott DJ, Harding SE, Rowe AJ (eds) Analytical ultracentrifugation. Techniques and methods. The Royal Society of Chemistry, Cambridge, pp 210–230

Hamer JE, Talbot NJ (1998) Infection-related development in the rice blast fungus *Magnaporthe grisea*. Curr Opin Microbiol 1:693–697. doi:10.1016/S1369-5274(98)80117-3

Hektor HJ (2005) Hydrophobins: proteins with potential. Curr Opin Biotechnol 16:434–439. doi:10.1016/j.copbio.2005.05.004

Kershaw MJ, Talbot NJ (1998) Hydrophobins and repellents: proteins with fundamental roles in fungal morphogenesis. Fungal Genet Biol 23:18–33. doi:10.1006/fgbi.1997.1022

Kwan AH, Macindoe I, Vukasin PV, Morris VK, Kass I, Gupte R, Mark AE, Templeton MD, Mackay JP, Sunde M (2008) The Cys3-Cys4 loop of the hydrophobin EAS is not required for rodlet formation and surface activity. J Mol Biol 382:708–720. doi:10.1016/j.jmb.2008.07.034

Linder MB, Szilvay GR, Nakari-Setala T, Penttila ME (2005) Hydrophobins: the protein-amphiphiles of filamentous fungi. FEMS Microbiol Rev 29:877–896. doi:10.1016/j.femsre.2005.01.004

Lucassen-Reynders EH (1981) Surfactant science series: anionic surfactants. In: Physical chemistry of surfactant action, vol 11. Marcel Dekker, New York, pp 173–216

Lugones LG, Wosten HAB, Birkenkamp KU, Sjollema KA, Zagers J, Wessels JGH (1999) Hydrophobins line air channels in fruiting bodies of *Schizophyllum commune* and *Agaricus bisporus*. Mycol Res 103:635–640. doi:10.1017/S0953756298007552

Lumsdon SO, Green J, Stieglitz B (2005) Adsorption of hydrophobin proteins at hydrophobic and hydrophilic interfaces. Colloids Surf B Biointerfaces 44:172–178

Ma H, Snook LA, Tian C, Kaminskyj SGW, Dahms TES (2006) Fungal surface remodelling visualized by atomic force microscopy. Mycol Res 110(Part 8):879–886. doi:10.1016/j.mycres.2006.06.010

Ma A, Shan L, Wang N, Zheng L, Chen L, Xie B (2007) Characterization of a *Pleurotus ostreatus* fruiting body-specific hydrophobin gene, Po.hyd. J Basic Microbiol 47:317–324. doi:10.1002/jobm.200710317

Ma AM, Shan LJ, Wang HJ, Du ZP, Me BJ (2008) Partial characterization of a hydrophobin protein Po.HYD1 purified from the oyster mushroom *Pleurotus ostreatus*. World J Microbiol Biotechnol 24:501–507

Mächtle W, Börger L (2006) Analytical ultracentrifugation of polymers and nanoparticles. Springer, Heidelberg

Myrvold R, Hansen FK (1998) Surface elasticity and viscosity from oscillating bubbles measured by automatic axisymmetric drop shape analysis. J Colloid Interface Sci 207:97–105. doi:10.1006/jcis.1998.5745

Ohnishi S, Tochio N, Tomizawa T, Akasaka R, Harada T, Seki E, Sato M, Watanabe S, Fujikura Y, Koshiba S, Terada T, Shirouzu M, Tanaka A, Kigawa T, Yokoyama S (2008) Structural basis for controlling the dimerization and stability of the WW domains of an atypical subfamily. Protein Sci 17:1531–1541. doi:10.1110/ps.035329.108

Penas MM, Rust B, Larraya LM, Ramirez L, Pisabarro AG (2002) Differentially regulated, vegetative-mycelium-specific hydrophobins of the edible basidiomycete *Pleurotus ostreatus*. Appl Environ Microbiol 68:3891–3898. doi:10.1128/AEM.68.8.3891-3898.2002

Schuck P (2005) Diffusion-deconvoluted sedimentation coefficient distribution for the analysis of interacting and non-interacting protein mixtures. In: Scott DJ, Harding SE, Rowe AJ (eds) Analytical ultracentrifugation. Techniques and methods. The Royal Society of Chemistry, Cambridge, pp 26–49

Stöhr J, Weinmann N, Wille H, Kaimann T, Nagel-Steger L, Birkmann E, Panza G, Prusiner SB, Eigen M, Riesner D (2008) Mechanisms of prion protein assembly into amyloid. Proc Natl Acad Sci USA 105:2409–2414. doi:10.1073/pnas.0712036105

Stroud PA, Goodwin JS, Butko P, Cannon GC, McCormick CL (2003) Experimental evidence for multiple assembled states of Sc3 from *Schizophyllum commune*. Biomacromolecules 4:956–967. doi:10.1021/bm034045e

Sunde M, Kwan AHY, Templeton MD, Beever RE, Mackay JP (2008) Structural analysis of hydrophobins. Micron 39:773–784. doi:10.1016/j.micron.2007.08.003

van der Vegt W, van der Mei HC, Wosten HAB, Wessels JGH, Busscher HJ (1996) A comparison of the surface activity of the fungal hydrophobin SC3p with those of other proteins. Biophys Chem 57:253–260

Van Wetter MA, Wosten HAB, Wessels JGH (2000) SC3 and SC4 hydrophobins have distinct roles in formation of aerial structures in dikaryons of *Schizophyllum commune*. Mol Microbiol 36:201–210. doi:10.1046/j.1365-2958.2000.01848.x

Walker N, Marcinowski S, Hillen H, Mächtle W, Jones Y, Stuart D (1990) Crystallization of human tumor necrosis factor. J Cryst Growth 100:168–179

Wang XQ, Graveland-Bikker JF, De Kruif CG, Robillard GT (2004) Oligomerization of hydrophobin SC3 in solution: from soluble state to self-assembly. Protein Sci 13:810–821

Wenta N, Strauss H, Meyer S, Vinkemeier U (2008) Tyrosine phosphorylation regulates the partitioning of STAT1 between different dimer conformations. Proc Natl Acad Sci USA 105:9238–9243

Wessels JGH (1994) Developmental regulation of fungal cell wall formation. Annu Rev Phytopathol 32:413–457

Wessels JGH (1997) Hydrophobins: proteins that change the nature of the fungal surface. Adv Microb Physiol 38:1–45

Wessels JGH (2000) Hydrophobins, unique fungal proteins. Mycologist 14:153–159

Whiteford JR, Spanu PD (2002) Hydrophobins and the interactions between fungi and plants. Mol Plant Pathol 3:391–400

Wiesehan K, Stohr J, Nagel-Steger L, van Groen T, Riesner D, Willbold D (2008) Inhibition of cytotoxicity and amyloid fibril formation by a D-amino acid peptide that specifically binds to Alzheimer's disease amyloid peptide. Protein Eng Des Sel 21:241–246

Wosten HAB (2001) Hydrophobins: multipurpose proteins. Annu Rev Microbiol 55:625–646

Wosten HAB, Van Wetter MA, Lugones LG, Van der Mei HC, Busscher HJ, Wessels JGH (1999) How a fungus escapes the water to grow into the air. Curr Biol 9:85–88